Pergamon

Int. J. Heat Mass Transfer. Vol. 39, No. 12, pp. 2485–2494, 1996

0017-9310/96 $15.00 + 0.00

0017-9310(95)00321-5

Direct simulations of turbulent unstratified natural convection in a vertical slot for $Pr = 0.71$

J. R. PHILLIPS

Fluid Dynamics Group, Pacific Northwest Laboratory, Richland, WA 99352, U.S.A.

(*Received* 29 *December* 1994 *and in final form* 23 *August* 1995)

Abstract—Turbulent unstratified natural convection in a vertical slot geometry is computed by integrating the unsteady three-dimensional Navier–Stokes equations. In the simulations no turbulence model is required and all the essential scales of turbulent motion are resolved. A large multiprocessor distributed memory computer is used, with satisfactory parallel efficiency, to simulate problems with up to 5 million grid points. Steady statistics are computed for Grashof numbers of 64 800 and 180 000. The corresponding Nusselt numbers computed for the two cases are 2.22 and 3.36. Turbulence statistics are computed for each case. Copyright © 1996 Elsevier Science Ltd.

INTRODUCTION

The various cases of natural convection in a slot have been studied extensively. If the slot walls are placed normal to the direction of gravity, the flow is referred to as Rayleigh–Bénard convection which is ubiquitous in the literature. If the slot walls are placed parallel to the direction of gravity, it is referred to as vertical slot convection. In between these two limiting cases there are arbitrary angle problems which have been studied in connection with solar panel design.

In 1909 Nusselt performed the first experiment measuring vertical slot convection heat transfer. This experiment was followed by several others, most attempting to correlate the Nusselt number to the Grashof or Rayleigh number, the Prandtl number and the aspect ratio. Later, Eckert and Carlson [1] performed experiments using a Zehnder–Mach interferometer to quantitatively image the vertical slot convection temperature field. They observed many of the important flow regimes common to vertical slot convection namely, the laminar conduction, transition, boundary layer, and travelling wave states. Apparently they did not observe the steady multicellular state but some turbulent states were observed.

In two papers by Elder [2, 3] laminar and turbulent vertical slot convection experiments are reported. In the laminar studies, Elder observed the steady multicellular state and the tertiary flow which occurs between the secondary flow structures. In Elder's turbulence studies he discovered that in the turbulent region centered at about mid-height of the geometry, there is a complete absence of the vertical temperature gradient commonly associated with the laminar flow regions. In Elder's geometry, stratification played little if any role in the physics of the turbulent region even though the effect of stratification was considerable in the laminar flow regions.

A more recent experimental paper by Chen and Wu [4] on vertical slot convection focused on the complication of temperature dependent viscosity. If this effect is taken into consideration, the antisymmetry of the problem is broken, resulting in a host of effects such as displacement of instability toward the hot wall and greater stability near the cold wall along with new varieties of unsteady laminar instabilities. Even though these effects are interesting it is likely that air flows at temperature differences commonly encountered would be affected very little by temperature–viscosity interactions and even less so when the flow becomes turbulent and mixing tends to make the temperature more uniform across the core of the flow. Chen and Wu also raise the important issue of the existence of three-dimensional unsteady laminar states in their paper.

Stability of the simple one-dimensional conduction state for vertical slot convection has received some attention in the literature. Of the studies that have been conducted probably the most precise computations for the unstratified case were carried out by Ruth [5] who gives seven figure values for the critical Grashof numbers and four figure values for the most unstable spatial wave numbers over a range of Prandtl numbers. At a Prandtl number of 0.7, the critical Grashof number is 8041 and the most unstable wave number is 2.81, where both are normalized by the slot thickness.

Perhaps the most complete set of stability calculations for the vertical slot problem to date is presented by Bergholz [6]. In his calculations he considered a range of Prandtl numbers and the influence of stratification. The effect of stratification can become important for many cases of the vertical slot

NOMENCLATURE

$\hat{\mathbf{e}}_x$ unit normal vector in the x-direction
E_{uu}, E_{vv}, E_{ww} one-dimensional energy spectra of fluctuating dimensionless velocity components
g gravitational acceleration
Gr Grashof number, $g\beta\Delta T(Y/2)^3/\nu^2$
Gr_Y Grashof number, $g\beta\Delta TY^3/\nu^2$
h heat transfer coefficient
k_x x-wave numbers, $Y\pi j/X$, $j = 0, 1, 2, \ldots$
k_z z-wave numbers, $Y\pi j/Z$, $j = 0, 1, 2, \ldots$
Nu Nusselt number, $h(Y/2)/\kappa$
Nu_Y Nusselt number, hY/κ
p dimensionless fluctuating pressure component
Pr Prandtl number, ν/α
t dimensionless time
T time-averaged dimensionless temperature
U time-averaged dimensionless velocity
$\mathbf{U}$ dimensionless velocity vector
uv dimensionless Reynolds shear stress
u^2, v^2, w^2 dimensionless Reynolds normal stresses
vt dimensionless velocity–temperature correlation
x, y, z dimensionless coordinates
X length of periodic slot domain in x-dimension
Y slot thickness in y-dimension
Z length of periodic slot domain in z-dimension.

Greek symbols
α thermal diffusivity
β thermal expansion coefficient
ΔT temperature difference across slot
Θ dimensionless temperature
κ thermal conductivity
ν kinematic viscosity.

problem. In particular, cases in which the aspect ratio of the enclosure is not large and the flow is laminar may have significant stratification effects. Cases other than these represent a large class of problems in which stratification plays a diminished role.

Early calculations of two-dimensional steady vertical slot convection using a finite difference method were carried out by Elder [7]. In these solutions, the basic unicellular flow state for stratified convection in a rectangular enclosure with an aspect ratio less than or equal to four was calculated for various conditions. Elder speculated that a loss of stability in his numerical scheme at higher Rayleigh numbers corresponded to experimentally observed secondary instabilities. De Vahl Davis [8] computed similar flows in a square enclosure with greater emphasis on the distributions of momentum source terms in the equations of motion. In Elder's paper [7] and De Vahl Davis' paper [8] the equations of motion were scaled using the Rayleigh and Prandtl numbers rather than the Grashof and Prandtl numbers. There has been some debate over the years as to which normalization is superior and it does not appear that an agreement has been reached on the subject.

De Vahl Davis [8] noted that as the Prandtl number was increased (all other parameters held constant), his simulation method became increasingly stable. After examining the form of his motion equations it is likely that this increased stability is actually the result of a decrease in normalized momentum diffusion (Grashof number) since the Rayleigh number is held constant while the Prandtl number is increased. Therefore, the amount of normalized thermal diffusion in the solution stays constant while the normalized momentum diffusion decreases leading to greater flow stability.

Korpela *et al.* [9] performed finite difference simulations of vertical slot convection in a two-dimensional rectangular enclosure using a finite difference method for aspect ratios up to 20. In these calculations, the equations were normalized using the Grashof number and the Prandtl number was held constant at 0.71. Results of the simulations were used to develop an expression for the optimal aspect ratio for a given Grashof number such that the Nusselt number is minimal. It is also noted in the paper that simulation of a very large aspect ratio would be of value when considering the heat transfer across double-glazed windows for commercial buildings.

Lee and Korpela [10] extended the simulations of Korpela *et al.* [9] to various aspect ratios, several Grashof numbers, and three Prandtl numbers. In this paper, an aspect ratio of 25 was reached showing the development of a central region controlled by multicellular flow once the critical Grashof number is exceeded. This larger aspect ratio simulation was at Prandtl number of 7 and Grashof number up to 40 000. At such high values, it is possible that three-dimensional motions might exist rendering the two-dimensional model inadequate.

EQUATIONS OF MOTION

Figure 1 depicts the normalized physical domain for the simulations. Within this domain the mathematical model is the unsteady three-dimensional incompressible Navier–Stokes equations with constant ther-

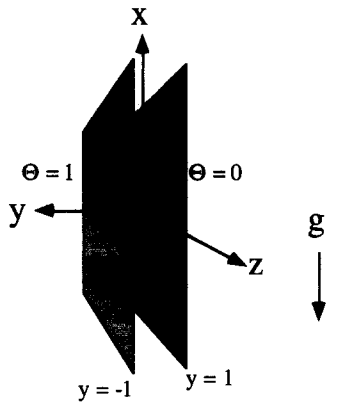

Fig. 1. Schematic diagram of the normalized physical domain.

mophysical properties with the Boussinesq approximation representing the buoyancy force term. Volumetric radiative heating of the gas is neglected. The dimensionless model equations are:

$$\nabla \cdot \mathbf{U} = 0 \tag{1}$$

$$\partial_t \mathbf{U} = \frac{1}{\sqrt{Gr}} \nabla^2 \mathbf{U} - \nabla\left(p + \frac{\mathbf{U}\cdot\mathbf{U}}{2}\right) + \mathbf{U} \times \boldsymbol{\omega} + (\Theta - \tfrac{1}{2})\hat{\mathbf{e}}_x \tag{2}$$

$$\partial_t \Theta = \frac{1}{Pr\sqrt{Gr}} \nabla^2 \Theta - \nabla \cdot \mathbf{U}\Theta \tag{3}$$

where $\boldsymbol{\omega} = \nabla \times \mathbf{U}$. The boundary conditions are

$$\mathbf{U}(y = \pm 1, t) = 0 \tag{4}$$

$$\Theta(y = 1, t) = 0 \tag{5}$$

$$\Theta(y = -1, t) = 1. \tag{6}$$

The remainder of the boundary conditions are periodic. Periodic boundary conditions require that the convection be unstratified since the time-averaged temperature along the direction of gravity is constant. The laminar initial conditions are:

$$\Theta(y, t = 0) = \tfrac{1}{2}(1 - y) \tag{7}$$

$$\mathbf{U}(y, t = 0) = \frac{\sqrt{Gr}}{12}(y^3 - y)\hat{\mathbf{e}}_x. \tag{8}$$

All equations are normalized using an inviscid convection velocity scale, $\sqrt{[g\beta\Delta T(Y/2)]}$, a length scale equal to half the slot thickness, $Y/2$, and a linear temperature normalization such that the high temperature is one and the low temperature is zero. This scaling is assumed in this article unless otherwise indicated.

In order to excite a turbulent state given a set of supercritical control parameters (Gr, Pr), a three-dimensional velocity or temperature disturbance must be added to the initial condition. This perturbation, which is on the order of 10^{-4} when compared to the basic state magnitude of 1, takes the place of small vibrations and natural kinetic fluctuations present in the laboratory flow. The perturbed flow must 'spin up' until it reaches a statistically steady turbulent state.

NUMERICAL METHOD

The model equations are approximated using the approach of Kim *et al.* [11]. Equations (1) and (2) are rewritten in a normal vorticity, ω_y, Laplacian of normal velocity, $\nabla^2 v$, form. This transformation eliminates the fluctuating pressure gradient term which is often expensive to compute. The time derivatives in the equations of motion are approximated using a third order semi-implicit Runge–Kutta scheme [12]. The fourth order equation for normal velocity is rewritten as two second-order equations which are solved in the usual manner as a linear combination of a homogeneous solution and two particular solutions to satisfy the resulting two-point boundary value problem.

The spatial derivatives are approximated using spectral basis functions constructed from complex Fourier series and Chebyshev polynomials. Boundary values are satisfied using Tau projection. The resulting linear systems are dense but can be reduced to tri-diagonal systems by reordering using recursion relations [13]. The standard convolution theorem approach is used to compute the spectral approximations of the nonlinear terms using "3/2 rule" high frequency filtering to remove aliasing in the unbounded directions.

The computations were carried out on the Intel Touchstone Delta computer at Caltech. The Intel Delta computer has a distributed memory, message passing architecture. The unit processor is the Intel i860 CPU which has a theoretical peak computation speed of 80 MFLOPS for single precision calculations ('well-written' Fortran code may achieve 10–30 MFLOPS single precision). The CPUs are each situated on a card with a high speed network processor and 16 MBytes of volatile memory. This card is referred to as an iPSC/860 numeric node. The configuration currently in use has 512 numeric nodes for a single precision theoretical peak machine speed of 40 GFLOPS. The numeric nodes are arranged in a 32×16 rectangular communication mesh with large mass storage units connected to various service nodes.

The algorithm was chosen for these calculations as a result of its natural ability to be mapped onto a message passing architecture in addition to its ideal numerical properties. Every step in the above algorithm can be mapped onto the Delta computer in a way which requires an extremely small amount of communication between numeric nodes. The only exception to this optimal situation is the three-dimensional FFT step. Since the algorithm and data base are mapped onto the numeric nodes in equal blocks of z-planes, the x- and y-direction transforms are entirely parallel. However, the z-direction transform requires that the entire data base be transposed across the mesh

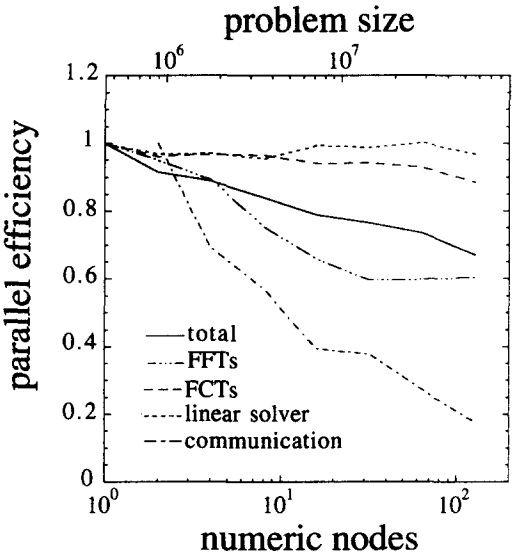

Fig. 2. Parallel efficiency of the scaled algorithm running on the Intel Touchstone Delta computer.

since the z transforms must be computed on a data structure which is stride one in order to be efficient. The transpose requires a global communication so that all numeric nodes involved in the simulation are sending and receiving data simultaneously thereby eliminating idle processor time. An algorithm for this transpose which performs satisfactorily on the rectangular mesh architecture is referred to as the optimal circuit switched algorithm [14].

Several timing cases with up to 128 numeric nodes were run to test the scaling behaviour of the algorithm implementation. Figure 2 shows the parallel efficiency of problems ranging in size from 456 192 to 57 065 472. The problem size is defined as three times the number of collocation grid points given that v, ω_y and Θ must be computed at each grid point. The performance of the code on scaled problems is satisfactory with no apparent asymptote in performance reached by 128 numeric nodes. Also shown are the performance of major components of the algorithm. An efficiency of one is ideal performance (perfect scaling). Efficiency is defined as the time to solution for a fixed number of time steps on a single numeric node divided by the time to solution of the scaled problem on multiple numeric nodes (each numeric node has a constant problem size). Counter-intuitively, the time advancement (linear solver) portion of the algorithm is more efficient when mapped onto larger numbers of numeric nodes. The overall parallel efficiency of the code is about 67% at 128 numeric nodes.

RESULTS AND DISCUSSION

Given the chosen Prandtl number, the convecting gas is assumed to be either dry air or nitrogen at an average temperature of about 300 K and a temperature difference of less than 20 K. Under these conditions, assuming dry air, volumetric radiative heating could account for as much as 0.7% of the total heat flux, surface to surface radiation could account for as much as 70% of the total heat flux, and convection would account for the remainder. The surface to surface radiation is uncoupled from the convection since it does not influence the gas or the isothermal boundary values. This estimated heat flux budget indicates that, in the case of dry air, neglecting volumetric radiative heating of the gas should result in less than a 3% flux deficit between the convection simulation and measured laboratory conditions. In the case of dry nitrogen, volumetric radiative heating could be ignored entirely. At these temperatures, assuming constant transport properties results in roughly a 1% error and the Boussinesq approximation has a truncation error of 0.1%.

Neglecting the effects of volumetric radiative heating and variable transport properties may have some minor influence on the calculated turbulence statistics, but computing these effects would have a substantial negative impact on the simulation's time to solution. Furthermore, since higher order terms in the body force expansion do not play a significant role under the given circumstances, use of the Boussinesq approximation is completely appropriate.

Under the above conditions, the slot thickness would be about 4 cm for a Grashof number of 22 500. This represents a fairly large, low temperature physical system, given the large aspect ratio required to minimize local stratification effects. If the surfaces can be maintained in an isothermal state for such a large system, the measurements are limited to the fully turbulent region, and the instrumentation is reasonably accurate and non-intrusive, laboratory measurements should be comparable to the turbulence statistics presented herein.

Simulations of turbulent flow were computed at Grashof numbers of 8100 and 22 500. In both cases the normalized physical domain had dimensions of $-2\pi \leqslant x \leqslant 2\pi$, $-1 \leqslant y \leqslant 1$, $-\pi \leqslant z \leqslant \pi$. The $Gr = 8100$ case had a computational domain with $84 \times 65 \times 64$ modes and $128 \times 65 \times 96$ grid points. The $Gr = 22\,500$ case had a computational domain with $128 \times 129 \times 128$ modes and $192 \times 129 \times 192$ grid points.

The resolution of the grid is deemed adequate if the computed one-dimensional energy spectra extend over several energy decades. Figure 3 shows the spectra in the x and z wave numbers, respectively. The minimum energy span is more than five decades and the maximum energy span is more than 10 decades. The resolution in the y direction is higher than in the x and z direction, particularly so in the near wall region as a result of the cosine mapping of the grid points. This level of resolution is considered adequate to resolve the essential scales of the turbulent motion.

To understand the mean properties of turbulent vertical slot convection, time-averaged statistics are computed. These include the mean velocity and tempera-

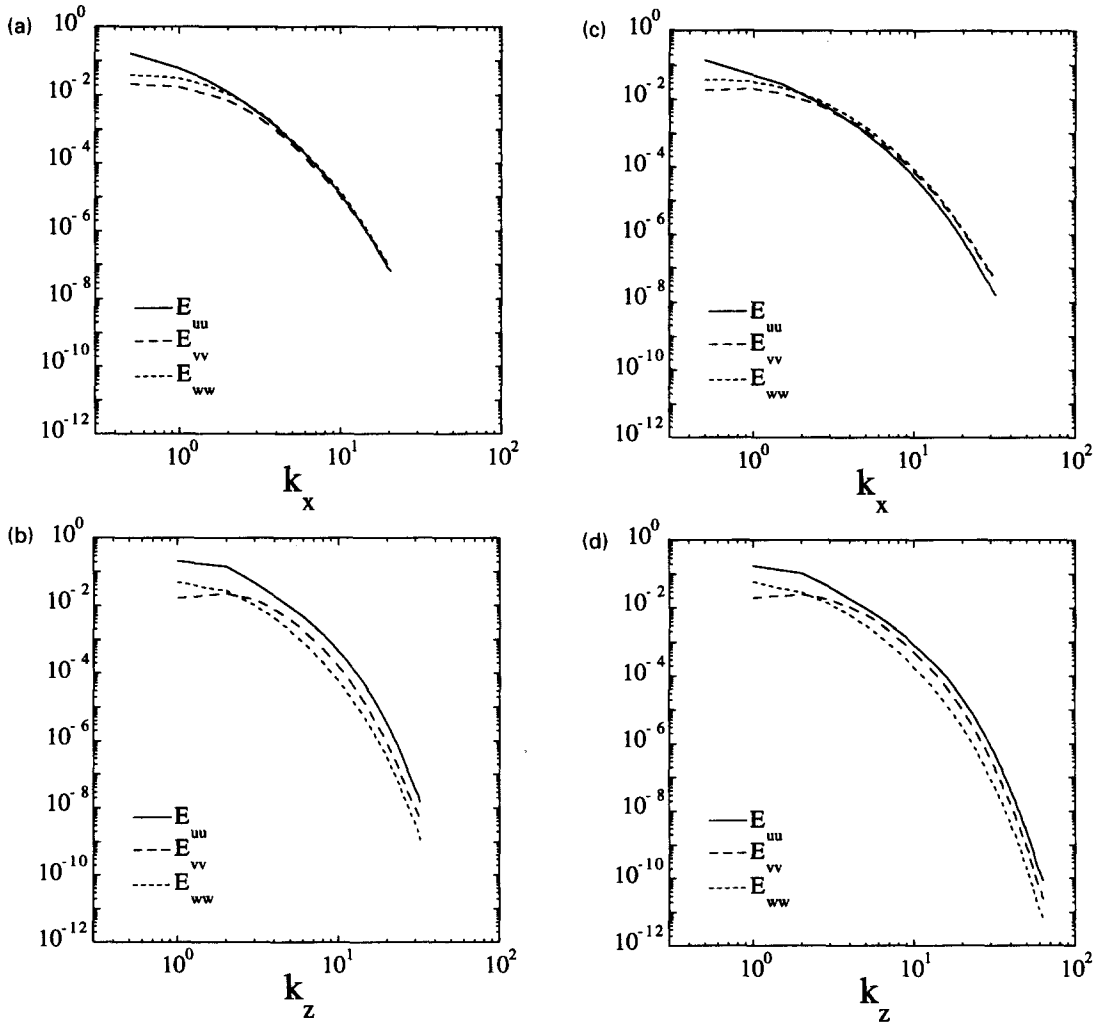

Fig. 3. One-dimensional energy spectra of the fluctuating velocity components. (a) x-spectra for $Gr = 8100$. (b) z-spectra for $Gr = 8100$. (c) x-spectra for $Gr = 22\,500$. (d) z-spectra for $Gr = 22\,500$.

ture, the mean velocity and temperature gradients, the non-zero components of the Reynolds stress tensor, the velocity–temperature correlation, and the temperature variance. These statistics are sampled by time-averaging the space-averaged values on homogeneous y-planes. The sample size is effectively doubled again by taking either symmetric or antisymmetric averages about the $y = 0$ plane since all the statistics are required by the time-averaged equations to have symmetric or antisymmetric solutions. Although the time-averaged flow variables are either symmetric or antisymmetric, the time-dependent flow variables have no symmetry properties which can be exploited.

The number of time steps required to calculate converged turbulence statistics depends on which statistic is being computed and the number of grid points in the y-planes. In the results presented here, a stationary state occurs after about 20 000 time steps and converged statistics required an addition 20 000–27 000 time steps to compute. Mean velocity and temperature profiles require fewer samples to converge than second order statistics. Normal Reynolds stress components u^2 and w^2 and the E_{uu} and E_{ww} spectra require the largest sample size to converge. CPU times required to compute converged statistics were about 26 h on 64 processors for the $Gr = 8100$ case and about 120 h on 128 processors for the $Gr = 22\,500$ case.

Figures 4(a) and (b) show the time-averaged velocity and temperature profiles for both Grashof numbers simulated. As expected, the velocity profile shows warm fluid rising and cool fluid falling with a flattened region in the slot center. The flattened region near the slot center is the result of the mean momentum contributions of the Reynolds shear stress and the mean temperature. As the Grashof number rises the y-coordinates of maximum fluid speed move closer to the boundaries at $y = -1, 1$. Mean temperature also behaves as expected with the center becoming flatter as the Grashof number increases. The flattened center region in this cases results from the action of the velocity–temperature correlation on mean thermal energy transport.

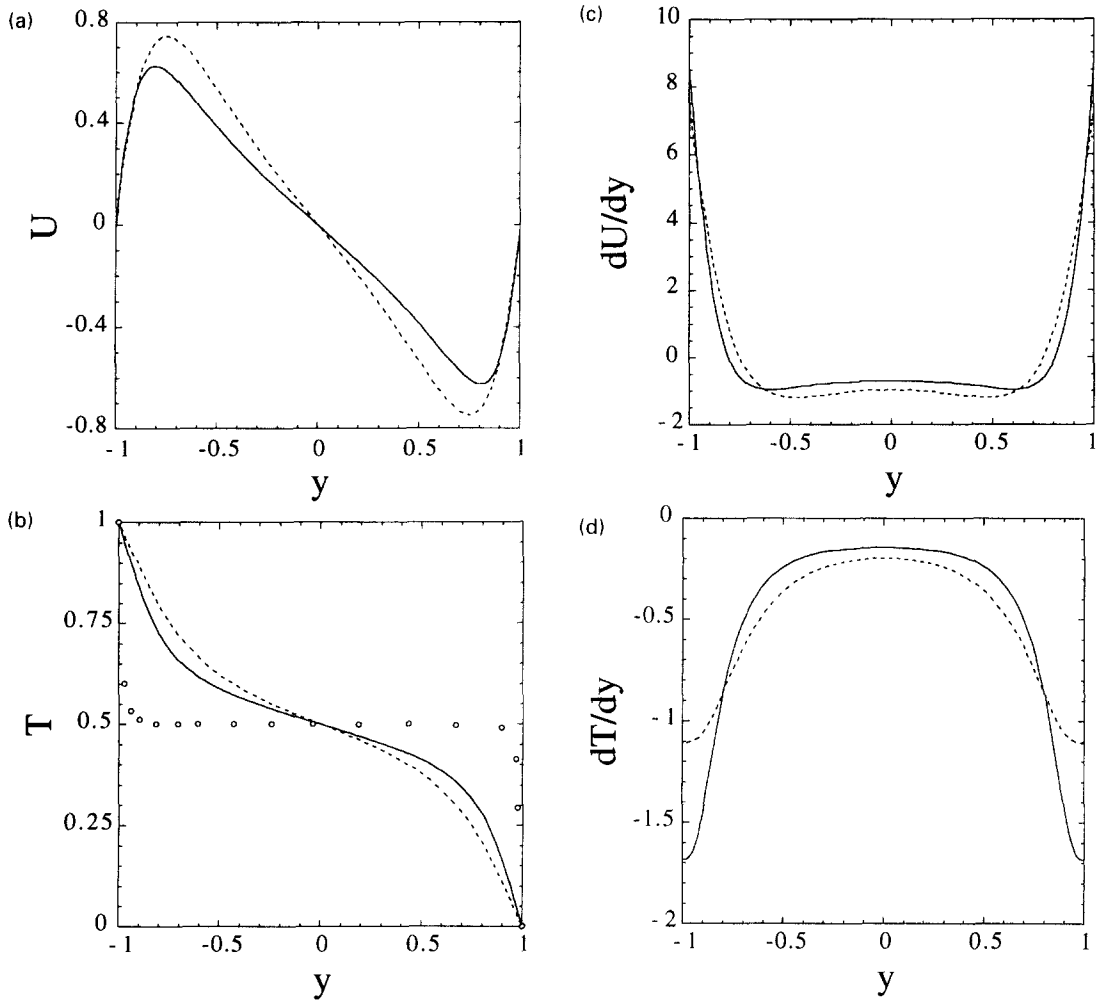

Fig. 4. (a) Time-averaged velocity profiles: dashed, $Gr = 8100$; solid, $Gr = 22\,500$. (b) Time-averaged temperature profiles: dashed, $Gr = 8100$; solid, $Gr = 22\,500$; Elder's [3] data points, $Gr = 4.1 \times 10^6$, $Pr = 7$. (c) Time-averaged velocity gradient profiles: dashed, $Gr = 8100$; solid, $Gr = 22\,500$. (d) Time-averaged temperature gradient profiles: dashed, $Gr = 8100$; solid, $Gr = 22\,500$.

In the interest of establishing the trend at higher Grashof numbers, the experimental time-averaged data of Elder [3] has been added to Fig. 4(b). Very little comparable data was found in the literature survey for the turbulent vertical slot convection problem. Existing comparable information in the literature is in the form of Nusselt number correlations and some time-averaged temperature data primarily at higher Prandtl numbers (for liquids). Turbulent vertical slot convection experiments, using dry air or nitrogen, collecting detailed turbulence statistics, represent a significant challenge. In particular, correlations involving the fluctuating normal velocity component such as uv and vt, would be extremely difficult to measure. Curiously, these two correlations are central to understanding the time-averaged transport of momentum and heat across the vertical slot.

Figures 4(c) and (d) show the time-averaged velocity and temperature gradients. As the Grashof number increases the mean gradients of the velocity and temperature move toward zero near the slot center while the magnitude of the gradients increases near the slot walls. The value of the normalized temperature gradient at the slot walls is the negative of the Nusselt number defined by the half slot thickness scale. The second derivative of the temperature gradient approaching zero at the slot wall indicates the existence of a viscous sublayer with a linear conduction heat transfer solution in the sublayer.

Figures 5(a)–(c) show the normal Reynolds stress components u^2, v^2 and w^2. Most of the energy is in the u^2 component followed by the w^2 and v^2 components. The v^2 component has a peak near the slot center and is weak near the slot walls. This indicates that the turbulence is primarily originating from the shear layer at the slot center as opposed to the boundary layers near the slot walls which are more stable. The hump which grows with increasing Grashof number at the center of the w^2 component may also indicate the dominance of the shear layer turbulence at the slot center.

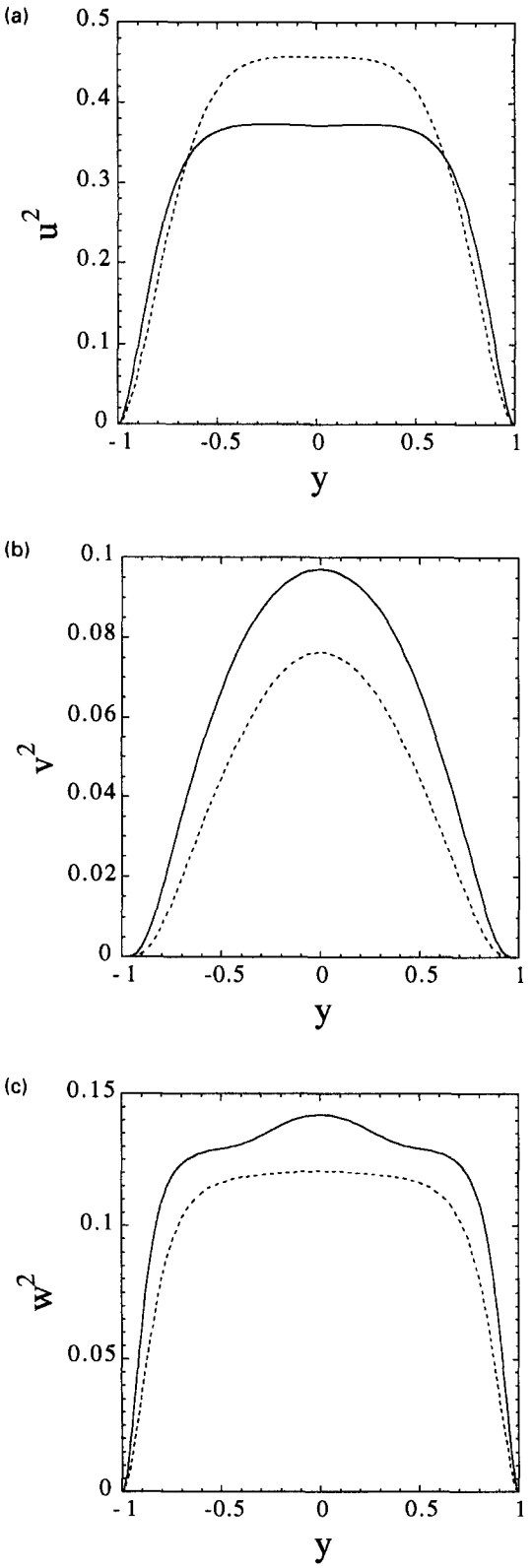

Fig. 5. (a) Normal Reynolds stress components, u^2: dashed, $Gr = 8100$; solid, $Gr = 22\,500$. (b) Normal Reynolds stress components, v^2: dashed, $Gr = 8100$; solid, $Gr = 22\,500$. (c) Normal Reynolds stress components, w^2: dashed, $Gr = 8100$; solid, $Gr = 22\,500$.

The Reynolds shear stress component, uv, and the velocity–temperature correlation, vt are shown in Figs. 6(a) and (b). These two components are active in the time-averaged equations of motion:

$$\frac{dU}{dy} - \left(\frac{dU}{dy}\right)_{y=-1} = \sqrt{Gr}\left\{uv - \int_{\tilde{y}=-1}^{y} (T-\tfrac{1}{2})\, d\tilde{y}\right\} \tag{9}$$

$$\frac{dT}{dy} - \left(\frac{dT}{dy}\right)_{y=-1} = Pr\sqrt{Gr}(vt) \tag{10}$$

where

$$Nu = -\left(\frac{dT}{dy}\right)_{y=-1}. \tag{11}$$

The Nusselt numbers and the mean velocity gradients at the slot walls are given in Table 1 normalized by the half slot thickness and, more traditionally, by the entire slot thickness. The computed Nusselt numbers are about 25% higher than commonly available correlations suggest but it is important to note that the correlations used are for aspect ratios less than 40. Since smaller aspect ratio enclosures have a turbulent region confined near the slot center away from the slot edges, the large laminar surrounding region would reduce the overall Nusselt number of the slot. The Nusselt numbers computed here should only be compared to Nusselt numbers measured locally in the turbulent region.

Useful relations can be derived from equations (9) to (11) by assuming the form of the asymptotic solution at sufficiently high Grashof and Prandtl numbers. Using the temperature data and observations of Elder [3] at $Gr = 4.1 \times 10^6$ and $Pr = 7$, and the implications of the calculations presented here, I assume that the mean velocity and temperature gradients are approaching zero at the slot center, then the relations follow:

$$\left(\frac{dU}{dy}\right)_{y=-1} \approx \sqrt{Gr}\left\{\int_{\tilde{y}=-1}^{0} (T-\tfrac{1}{2})\, d\tilde{y} - (uv)_{y=0}\right\} \tag{12}$$

$$Nu \approx Pr\sqrt{Gr}(vt)_{y=0}. \tag{13}$$

From these relations the shear stress at the slot walls can be estimated from a measured temperature profile and Reynolds shear stress at the slot center, and the velocity–temperature correlation at the slot center can be estimated from a measured Nusselt number if the Grashof and Prandtl numbers are sufficiently high.

The variance of the fluctuating temperature is shown in Fig. 6(c) to illustrate the region of strongest advective mixing with corresponding peaks and the depression in the slot center which results from the damping effect of thermal diffusion. Higher Prandtl number fluids would presumably have stronger temperature fluctuations in the slot center. In the limit of

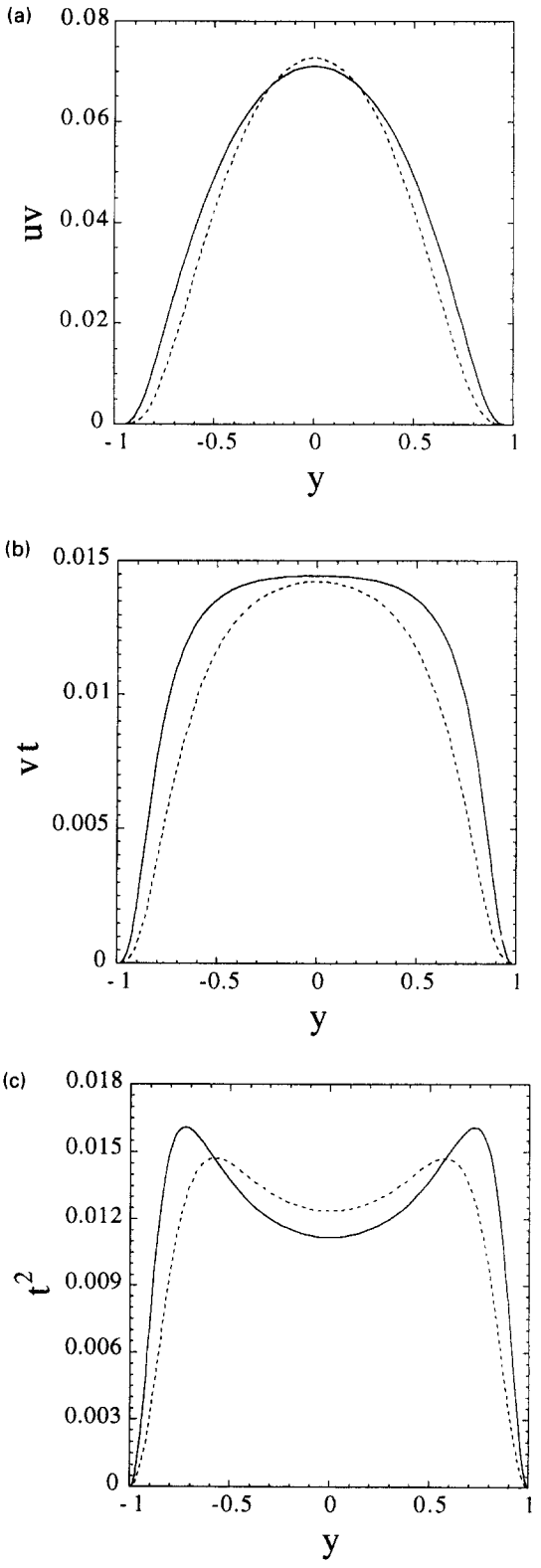

Fig. 6. (a) Reynolds shear stress components, uv: dashed, $Gr = 8100$; solid, $Gr = 22\,500$. (b) Velocity–temperature correlations, vt: dashed, $Gr = 8100$; solid, $Gr = 22\,500$. (c) Variances of fluctuating temperatures, t^2: dashed, $Gr = 8100$; solid, $Gr = 22\,500$.

Table 1. Computed Nusselt number and boundary velocity gradient for $Pr = 0.71$

Gr (Gr_Y)	8100(64 800)	22 500(180 000)
Nu (Nu_Y)	1.11(2.22)	1.68(3.36)
dU/dy (dU/dy_Y)	7.38(10.4)	8.56(12.1)

infinite Prandtl number the temperature probability distribution function is bimodal with temperature samples occurring only at zero and one with resulting intense temperature fluctuations. Zero Prandtl number would lead to zero temperature fluctuations everywhere.

Instantaneous turbulent flow structures can be visualized using isosurfaces of scalar variables. In Fig. 7(a) an isotherm at $\Theta = 1/2$ is shown for the $Gr = 8100$ case (visualized at an angle and in perspective for clarity). The two transparent gray planes represent the boundaries of the computational domain with the cool wall represented by the front plane with the x-axis directed upward along the longest side of the domain. Figure 7(b) shows the same isotherm for the $Gr = 22\,500$ case. The increase in the number of flow scales is obvious and the isotherm has appendages which penetrate closer to the slot walls.

The $Gr = 22\,500$ case also exhibits closed loops in its isotherms such as the one shown on the lower right-hand side of Fig. 7(b). These closed loops always seem to align in the average flow direction at this Grashof and Prandtl number and are distorted as they advect with the flow stream. Observations suggest that these loops are formed when a sufficiently energetic counter-rotating vortex pair in the mixing layer aligned in the mean flow direction forces fluid from the slot center toward a slot wall. As the fluid ejected away from the center approaches the slot wall, the structure thins and stretches creating a local high z-direction temperature gradient behind the structure. Since the Prandtl number is moderate the high temperature gradient diffuses away forming the closed loop in the isotherm. The $Gr = 8100$ case seems to lack the advective energetics required to form these closed loops.

CONCLUDING REMARKS

Unstratified turbulent natural convection in a vertical slot can be accurately simulated using direct simulation methods. Although the physics of laminar flow states are often complicated by stable stratification, experimental evidence strongly suggests that stratification is not physically significant for the turbulent flow state [3]. Even so, it is possible that in laboratory enclosure flows, stable stratification might delay the onset of turbulence to a somewhat higher Grashof number than expected in these calculations. Once a fully turbulent region is formed near the slot center, the stable stratification would relax in the turbulent region as a result of an initially strong streamwise velocity–temperature correlation. If the Grashof

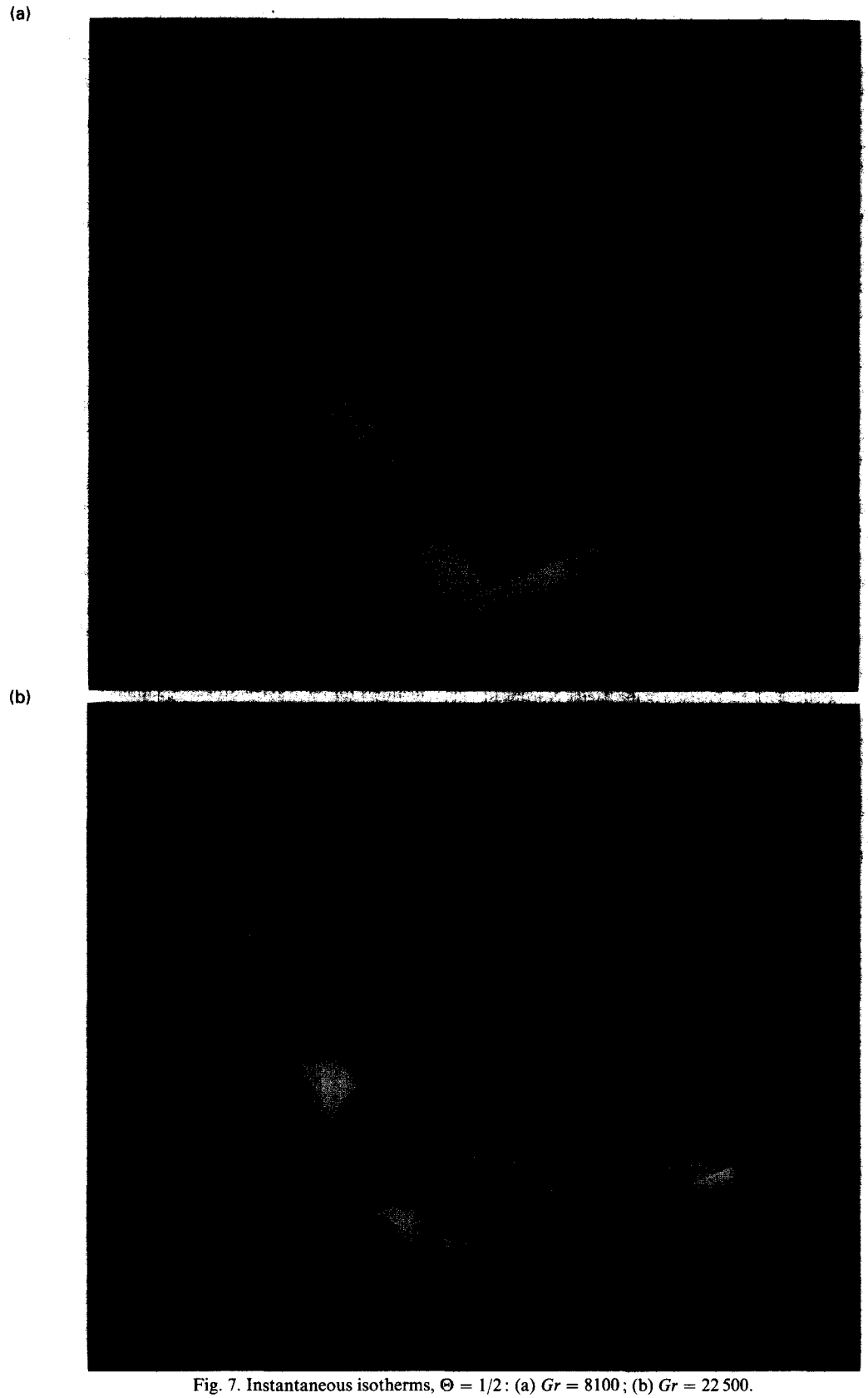

Fig. 7. Instantaneous isotherms, $\Theta = 1/2$: (a) $Gr = 8100$; (b) $Gr = 22\,500$.

number is reduced to a lower value at that point, one might expect subcritical turbulence to persist and stable stratification to remain absent since hysteresis in transitional flows is common.

For a Prandtl number of 0.71, the shear layer at the slot center transitions to a turbulent state first with the boundary layer becoming turbulent at a more elevated Grashof number. The existence of relatively thick laminar flow layers adjacent to the slot walls is evident in both the instantaneous solution and the turbulent flow statistics for the Grashof numbers computed. One might expect to see more significant turbulent boundary layer effects at higher Grashof numbers.

Further calculations exploring the effects of weak stratification on the streamwise velocity–temperature correlation would contribute some understanding of the mechanism which relaxes stable stratification in the turbulent flow. Calculations at a higher Grashof number would help establish the high Grashof number trends suggested by equations (12) and (13). And finally, calculations at arbitrary angles with respect to gravity would shed light on the turbulence properties of the unsymmetric cases.

Acknowledgements—The ichannel code and helpful comments on code modifications were provided by Dr Robert Moser of the NASA Ames Research Center. I would also like to acknowledge Dr Erik Pearson of the Pacific Northwest Laboratory for helping to secure funding for this research. This research was performed in part using the Intel Touchstone Delta computer operated by Caltech on behalf of the Concurrent Supercomputing Consortium. Access to this facility was provided by the Pacific Northwest Laboratory. The Pacific Northwest Laboratory is operated for the U.S. Department of Energy by Battelle Memorial Institute under contract DE-AC06-76RL01830.

REFERENCES

1. E. R. G. Eckert and W. O. Carlson, Natural convection in an air layer enclosed between two vertical plates with different temperatures, *Int. J. Heat Mass Transfer* **2**, 106–120 (1961).
2. J. W. Elder, Laminar free convection in a vertical slot, *J. Fluid Mech.* **23**, 77–98 (1965).
3. J. W. Elder, Turbulent free convection in a vertical slot, *J. Fluid Mech.* **23**, 99–111 (1965).
4. F. Chen and C. H. Wu, Unsteady convective flows in a vertical slot containing variable viscosity fluids, *Int. J. Heat Mass Transfer* **36**(17), 4233–4246 (1993).
5. D. W. Ruth, On the transition to transverse rolls in an infinite vertical fluid layer—a power series solution, *Int. J. Heat Mass Transfer* **22**, 1199–1208 (1979).
6. R. F. Bergholtz, Instability of steady natural convection in a vertical fluid layer, *J. Fluid Mech.* **84**(4), 743–768 (1978).
7. J. W. Elder, Numerical experiments with free convection in a vertical slot, *J. Fluid Mech.* **24**(4), 823–843 (1966).
8. G. De Vahl Davis, Laminar natural convection in an enclosed rectangular cavity, *Int. J. Heat Mass Transfer* **11**, 1675–1693 (1968).
9. S. A. Korpela, Yee Lee and J. E. Drummond, Heat transfer through a double-pane window, *J. Heat Transfer* **104**, 539–544 (1982).
10. Yee Lee and S. A. Korpela, Multicellular natural convection in a vertical slot, *J. Fluid Mech.* **126**, 91–121 (1983).
11. J. Kim, P. Moin and R. D. Moser, Turbulence statistics in fully developed channel flow at low Reynolds number, *J. Fluid Mech.* **177**, 133–166 (1987).
12. P. R. Spalart, R. D. Moser and M. M. Rogers, Spectral methods for the Navier–Stokes equations with one infinite and two periodic directions, *J. Comp. Phys.* **96**, 297–324 (1991).
13. P. Moin and J. Kim, On the numerical solution of time-dependent viscous incompressible fluid flows involving solid boundaries, *J. Comp. Phys.* **35**, 381–392 (1980).
14. E. Jackson, Zhen-Su She and S. A. Orszag, A case study in parallel computing—I. Homogeneous turbulence on a hypercube, *J. Sci. Comput.* **6**(1), 27–45 (1991).